Available online at www.sciencedirect.com
SCIENCE DIRECT®
Journal of Solid State Chemistry 177 (2004) 389–394
JOURNAL OF SOLID STATE CHEMISTRY
http://elsevier.com/locate/jssc

On the electronic and structural properties of aluminum diboride $Al_{0.9}B_2$

Ulrich Burkhardt,[a,*] Vladimir Gurin,[a,b] Frank Haarmann,[a] Horst Borrmann,[a] Walter Schnelle,[a] Alexander Yaresko,[a] and Yuri Grin[a]

[a] *Max-Planck-Institut für Chemische Physik fester Stoffe, Nöthnitzer Straße 40, 01187 Dresden, Germany*
[b] *A. F. Ioffe Physico-Technical Institute, Russian Academy of Sciences, Politekhnicheskaya str. 26, 194021 St. Petersburg, Russia*

Received 14 November 2002; accepted 20 December 2002

Abstract

Single crystals of aluminum diboride (space group *P*6/*mmm*, No. 191) $a = 3.0050(1)$ Å, $c = 3.2537$ (8) Å; $Z = 1$) were prepared by the aluminum flux method. Crystal structure refinement shows defects at the aluminum site and resulted in composition $Al_{0.894(9)}B_2 \approx Al_{0.9}B_2$. The defect structure model is confirmed by the measured mass density $\rho_{exp} = 2.9(1)$ g/cm^3 in comparison with a calculated value $\rho_x = 3.17$ g/cm^3 for full occupancy of the aluminum position. The results of ^{11}B NMR measurements support the defect model and are in agreement with the structure obtained by X-ray diffraction methods. Electrical resistivity measured on a single crystal parallel to its hexagonal basal plane with $\rho(300\,K) - \rho(2\,K) = 2.35\,\mu\Omega$ cm shows temperature dependence like a typical metal. Charge is dominantly carried by holes (Hall-coefficient $R = +2 \times 10^{-11}$ m/C). Respective, p-type conductivity is confirmed by theoretical calculations. Chemical bonding in aluminum diboride is discussed using the electron localization function.

Keywords: Aluminum diboride; Defect crystal structure; Density; NMR measurements; Electrical resistivity; Hall-coefficient; Chemical bonding

1. Introduction

The aluminum-richest phase of the binary aluminum–boron system has been known for a long time and the corresponding structure type AlB_2 is one of those most frequently observed among intermetallic phases. The chemical variability and simplicity of the crystal structure with graphite-like nets of boron atoms separated by aluminum in hexagonal prismatic voids make this structure type a very interesting one for systematic investigation of crystal chemical and physical properties by experimental as well as theoretical methods. Important representatives of this structure type are transition metal diborides whose particular hardness and refractory properties are frequently applied. The discovery of superconductivity at $T = 39$ K in magnesium diboride [1] initiated a strong interest also in *s*–*p* diborides. Here, the in-plane boron–boron bonding plays a crucial role for the electron–phonon coupling but also for the electronic density of states near E_F. From a chemical point of view, six-membered rings with homonuclear bonding are well known not only for boron arrangements in intermetallic compounds but also for other elements of groups 13, 14 and 15 of the Periodic Table and are usually described as the polyanionic part of respective structures. The electronic stabilization of anions like $[Si_6]^{10-}$ by external atomic groups may be accompanied by the formation of complex superstructures [2]. Several variants with vacancies in the anionic partial structure are known.

In this context, our interest was raised by strongly varying data available in the literature on the very simple phase AlB_2. A first crystal structure determination by X-ray methods revealed hexagonal symmetry (space group *P*6/*mmm*) with complete occupation of both atomic positions according to composition AlB_2 [3]. However, density measurements [4, 5] indicated defects in the structure. Scarcely described chemical analyses gave different results: $Al_{1.0}B_2$ [6] or $Al_{0.9}B_2$ [4]. This motivated us to re-examine the crystal structure and to further characterize the phase by ^{11}B NMR, electrical resistivity and Hall-coefficient measurements.

*Corresponding author. Fax: ++49-351-4646-4002.
E-mail address: burkhardt@cpfs.mpg.de (U. Burkhardt).

0022-4596/$ - see front matter © 2003 Elsevier Inc. All rights reserved.
doi:10.1016/j.jssc.2002.12.001

Chemical bonding and electronic properties are discussed in the light of quantum chemical calculations.

2. Experimental

Preparation route 1: Single crystals suitable for X-ray investigation were separated from an aluminum-rich sample of nominal composition $Al_{98}B_2$ prepared by arc melting of a pressed pellet of aluminum and boron powders (purity grades: Al—99.99%; amorphous boron—99.9%). Slow precipitation of the aluminum diboride phase from the $Al_{98}B_2$ liquid was achieved near its peritectic temperature at 980°C (see phase diagram [7]).

Preparation route 2: Larger single crystals taken, e.g., for resistivity and Hall effect measurements were separated from a 70 g batch of an initial alloy of composition $Al_{97.7}B_{2.3}$. Here, the mixture (purity Al—99.9%, B—99.7%) was melted in a furnace under argon atmosphere using alumina crucibles. The melt was slowly cooled during 18 h from 1350°C to 660°C considering the reported phase diagram [7] to get well-facetted single crystals [8].

In both cases, excess aluminum was dissolved in diluted hydrochloric acid. The residues contain only crystals with pronounced hexagonal plate-like habit, some micrometers thick and with lateral dimensions up to few millimeters. All crystals show dark golden metallic lustre. The purity of the material was controlled by EDX analyses on several crystals. No additional elements besides aluminum and boron were found.

The crystal structure investigation was performed on a STOE STADI 4 diffractometer and on a Rigaku Raxis-RAPID diffraction system. All relevant details concerning data collection and crystallographic data are listed in Table 1. Unit-cell parameters were obtained from least-squares fits of Guinier powder data (Huber G670 Image Plate Camera, Cu$K\alpha_1$ radiation, $\lambda = 1.54060$ Å) using LaB_6 ($a = 4.15692$ Å) as internal standard.

The mass density was determined with a helium gas pycnometer (AccuPyc 1330, Micromeritics). The sample volume V was measured with an accuracy of 0.0001 cm^3. The corresponding mass of about 50 mg was determined with an absolute accuracy of 0.1 mg.

Electrical resistivity measurements were carried out on single crystalline material by a direct current four-probe method in a temperature range $1.8\,K < T < 300\,K$. Because of the pronounced plate-like habit of the single crystal (length $l = 850\,\mu m$, thickness $d = 10\,\mu m$), only resistivity values perpendicular to the crystallographic c-axis were determined (current flow direction along the [100] direction). Magnetic field sweeps to ± 5 T were applied to determine the Hall coefficient using the six-probe method. The external magnetic field was aligned parallel to the crystallographic c-axis. Hall voltage was measured parallel to the crystallographic [210] direction and perpendicular to the current flow.

Ambient temperature ^{11}B NMR experiments were done at a Bruker MSL 300 instrument ($B_0 = 7.05$ T) using purified powder samples of AlB_2 (Aldrich, X-ray purity). In order to prevent dead time delays spectra were accumulated applying Hahn echo pulse sequences. Due to the distinct width of the spectrum, only the narrow central transition could be detected in a single experiment without distortion of the line shape. The spectrum was measured with $\pi/2$ pulse length of

Table 1
Crystallographic data for $Al_{0.9}B_2$

	Crystal 1	Crystal 2
Crystal shape	Hexagonal prismatic 0.05 mm × 0.05 mm × 0.02 mm	Hexagonal prismatic 0.17 mm × 0.10 mm × 0.012 mm
Space group	*P6/mmm* (no. 191)	*P6/mmm* (no. 191)
Formula per unit cell	$Z = 1$	$Z = 1$
Unit-cell parameters	$a = 3.0050(1)$ Å	$a = 3.0050(1)$ Å
(powder data)	$c = 3.2537(8)$ Å	$c = 3.2537(8)$ Å
Volume	$V = 25.445(8)$ Å^3	$V = 25.445(8)$ Å^3
Data collection	STOE STADI 4 Mo$K\alpha$, $\lambda = 0.71069$ Å Graphite monochromator	Rigaku Raxis RAPID Mo$K\alpha$, $\lambda = 0.71069$ Å Graphite monochromator
No. of measured/unique reflections	624/50	792/128
Measured range	$2\theta_{max} = 80°$ $-5 \leqslant h \leqslant 5$ $-5 \leqslant k \leqslant 5$ $-5 \leqslant l \leqslant 5$	$2\theta_{max} = 140°$ $-7 \leqslant h \leqslant 7$ $-7 \leqslant k \leqslant 3$ $-4 \leqslant l \leqslant 8$
No. of reflections used for refinement [$F(hkl) > 2\sigma F(hkl)$]	50	125
No. of refined parameters	7	7
R_F	0.023	0.035
Software	WinCSD [27]	WinCSD [27]

2 μs. To analyze the undistorted line shape of the full spectrum, the frequency of the transmitter was varied in a range of ±1 MHz with respect to the reference frequency of $BF_3 \cdot (C_2H_5)_2O$. Pulses of 100 μs for $\pi/2$ were used to detect the individual echo spectra in order in to achieve sufficient resolution for the whole spectrum.

3. Results and discussion

3.1. Crystal structure determination

The crystal structure was refined using diffraction data of two crystals (one from each preparation route). Crystallographic information and data handling are presented in Table 1.

In case of crystal 1 (preparation route 1), an attempt to refine the structure with complete occupation of both positions (aluminum and boron) led to $R(F)_{iso} = 0.037$ in the isotropic and $R(F)_{aniso} = 0.027$ for the anisotropic approximation of atomic displacement. Despite quite acceptable values of the residual factors, the result showed an unexpected ratio in displacement parameters: U_{eq}(Al) was considerably larger than U_{eq}(B). A refinement of the site occupancy for the aluminum position (*SOF*(Al)) and subsequent refinement of atomic displacement parameters led to slightly smaller residual values ($R(F)_{iso} = 0.033$ and $R(F)_{aniso} = 0.023$) and an occupation factor *SOF*(Al) = 0.91(1), but with much more reasonable ratio of $U_{eq}(Al)/U_{eq}(B)$, see Table 2. Unfortunately, simultaneous refinement of displacement and occupation factors was unstable due to severe correlation of parameters and due to the limited data set. Detailed investigations on the isotypical phases TiB_2 and MgB_2 [9] have shown, that the displacement factor for the metal position should be only slightly larger than that for the boron position. Taking this into account, a second diffraction experiment on crystal 2 (route 2) was performed to much higher diffraction angles (Table 1). This experiment confirmed the results of the first one and converged for *SOF*(Al) = 0.878(8), see Table 2. With the large data set the simultaneous refinement of occupation and displacement parameters converged without difficulties. The slightly larger value of *R*(*F*) in the second experiment is due to the larger contribution of the weak reflections at higher diffraction angles. For reflections with $2\theta \leqslant 80°$, the value of *R*(*F*) is 0.025 in good agreement with 0.023 from the first experiment. Averaging of the results for both experiments gives *SOF*(Al) = 0.894(8).

Clear support for the defect model comes from mass density measurements carried out in a helium gas pycnometer. The mass density value $\rho_{exp} = 2.9(1)\ g/cm^3$ agrees well with $\rho_x = 2.98(2)\ g/cm^3$ as calculated on the basis of the defect structural model $Al_{0.894}B_2$, and is definitely smaller than the corresponding value $\rho_x = 3.17\ g/cm^3$ calculated for the fully occupied composition AlB_2. Other reported density data ($\rho = 2.84\ g/cm^3$ [4], $\rho = 2.955\ g/cm^3$ [3] are also compatible with defects at the aluminum position. Literature data on lattice parameter *c* vary from *c* = 324 pm [4] to *c* = 326.2(1) pm [8] and may be considered as indication of a small homogeneity range. In such a case composition $Al_{0.894}B_2 \approx Al_{0.9}B_2$ should represent the maximal aluminum content in the aluminum diboride phase, because of the preparation from the aluminum-rich melt.

Recently, composition $Al_{0.93}B_2$ was estimated from X-ray emission and absorption spectra [10] and $Al_{0.89}B_2$ was derived from high-pressure synchrotron powder diffraction data [11].

3.2. NMR investigation

The ^{11}B NMR spectrum is presented in Fig. 1. It is dominated by the electric quadrupolar coupling of the ^{11}B nuclei to the surrounding electric field gradient. The quadrupolar frequency can be estimated from the satellites to $\nu_Q = 540 \pm 20$ kHz which is in good agreement with earlier results [12,13]. The slight distortion of the spectrum in the region of the central transition is due to an anisotropy of the Knight shift which is in the order of $\Delta K \approx 130$ ppm. A small anisotropy of the Knight shift was predicted by ab initio calculations [13]. Neither an asymmetry of the quadrupolar coupling nor the Knight shift was observed ($\eta_Q = \eta_K = 0$). The absolute Knight shift of $\Delta K = -10 \pm 5$ ppm was determined by MAS measurements [13].

The calculated spectrum for $I = \frac{3}{2}$ using the values of ν_Q, η_Q, ΔK and η_K as mentioned above is presented in

Table 2
Atomic coordinates and displacement parameters U_{ij} [Å^2] for $Al_{0.9}B_2$. For both sites: $U_{11} = U_{22} = 2U_{12}$; $U_{13} = U_{23} = 0$. Upper line—crystal 1, lower line—crystal 2

Atom	Site	*x/a*	*y/a*	*z/c*	*SOF*	U_{eq}	U_{11}	U_{33}
A1	1*a*	0	0	0	0.91(1)	0.0055(2)	0.0063(3)	0.0039(4)
					0.878(8)	*0.00873(1)*	*0.0092(2)*	*0.0078(2)*
B	2*d*	1/3	2/3	1/2	1	0.0044(4)	0.0040(5)	0.0051(7)
					1	*0.0069(2)*	*0.0059(3)*	*0.0089(4)*

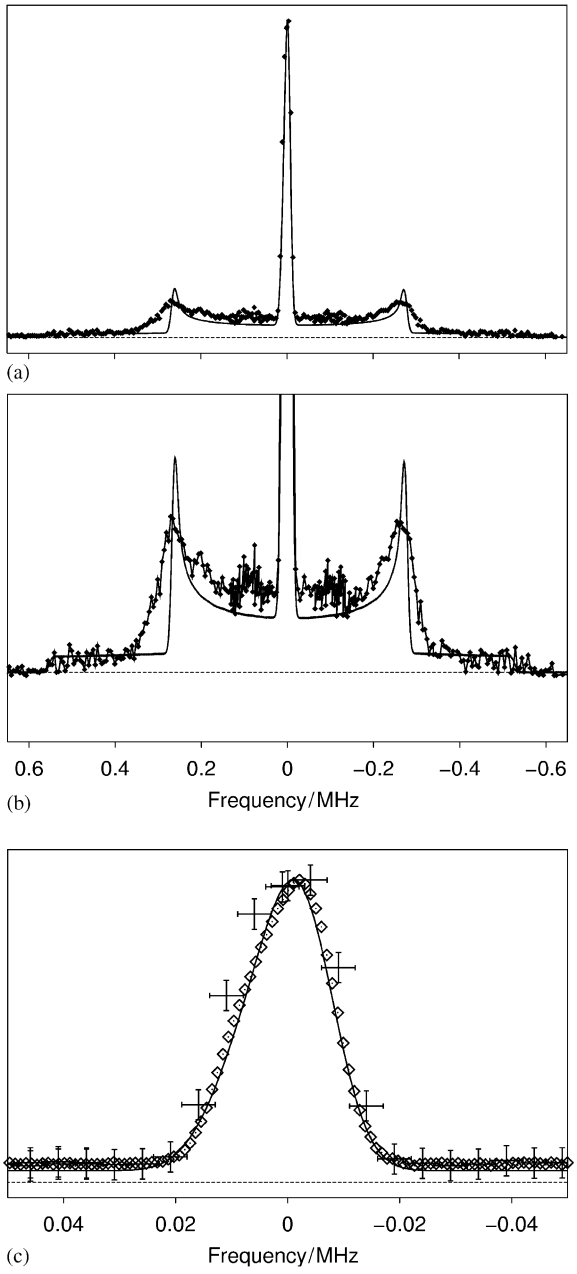

Fig. 1. (a) ^{11}B NMR spectrum of $Al_{0.9}B_2$: ♦, Hahn echo experiment; full line, calculated spectrum for $I=\frac{3}{2}$ with $\nu_Q=540$ kHz, $\eta_Q=0$ and $\Delta K=130$ ppm, $\eta_K=0$. (b) Magnification of subfigure (a). (c) ^{11}B NMR spectrum of the central transition for $Al_{0.9}B_2$; error bars, series of echo measurements; ◇, white line spectrum; full line, calculated spectrum.

Fig. 1a–c. We assume coincidence of the principal axis system for the Knight shift with quadrupolar interaction. This seems to be reasonable taking into account the results concerning chemical bonding (see Section 3.4. *Chemical bonding*). In first-order perturbation theory which is appropriate here the central transition is not influenced by quadrupolar contributions and therefore it is dominated by dipolar coupling and anisotropy of the Knight shift. The agreement of the observed and the calculated spectrum in the central transition region is good (Fig. 1c). Deviations in the calculated line shape of the satellites (Fig. 1b) are related to the distribution of quadrupolar frequencies which lead to the shape broadening. A similar effect was observed in the ^{27}Al NMR spectrum of AlB_2 [12].

In accordance with the results of the other experiments presented above, defects on the aluminum position producing different local environments of the boron atoms are the most probable reason for the observed distribution of quadrupolar frequencies.

3.3. Electrical properties and band structure

Electrical resistivity of $Al_{0.9}B_2$ in the basal plane of the hexagonal crystal shows (see *Experimental*) typical metallic behavior down to $T=1.8$ K (Fig. 2) with a rather small residual resistance ratio $RRR=\rho(293\,K)/\rho(4\,K)=1.4$. The measured values of the Hall coefficient R_H carry a positive sign and decrease on decreasing temperatures (Fig. 3). The low-temperature limit R_H $(T=4.2\,K)=+2\times10^{-11}\,m^3/C$ corresponds to $n=7.7$

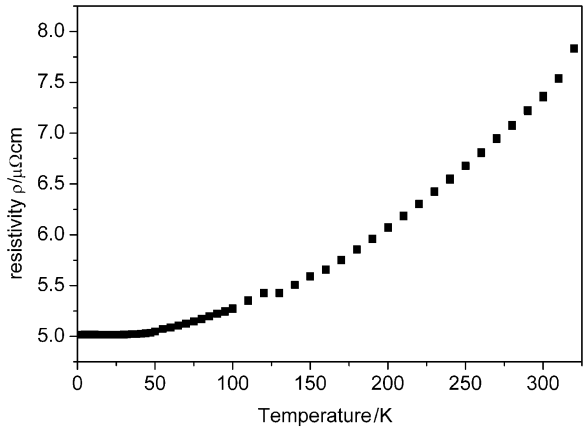

Fig. 2. Temperature dependence of the electrical resistivity parallel to the hexagonal basal plane of $Al_{0.9}B_2$.

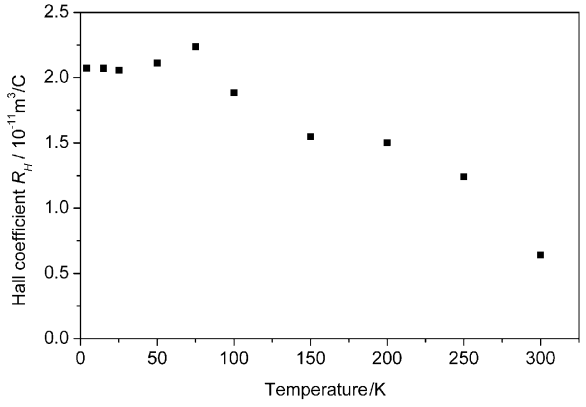

Fig. 3. Temperature dependence of Hall coefficient R_H determined from the measured Hall voltage perpendicular to the *a*-axis and in the basal plane of hexagonal AlB_2.

holes per unit cell assuming the very simplified one-band model with $n = 1/eR_H$. Nearly one hole per aluminum atom was reported from single-crystal Hall effect measurements at room temperatures [14]. However, definitely larger resistivity values of $\rho(293\,K) = 31$–$77\,\mu\Omega\,cm$ were observed in these experiments indicating lower quality of the material used.

The electronic structure of non-defect aluminum diboride was calculated using the local density functional approach (LDA) as implemented in the linear muffin–tin orbital (LMTO) method [15] and Tight–Binding LMTO program package [16]. The Hall coefficient tensor components were calculated on the basis of an approximate solution of the Boltzmann equation [17]. Electron velocities as introduced in the expressions for transport coefficients were obtained by numerical differentiation of energy bands calculated on a regular $48 \times 48 \times 48$ k-mesh [18]. The Fermi surface integrals were evaluated using the tetrahedron method [19]. The band structure (Fig. 4a) contains bands with strong dispersion crossing the Fermi level, in contrast to a relatively flat band structure as would be expected for graphite-like nets. This leads to a more complicated Fermi surface than assumed by the very simple one-band model applied for the interpretation of the experimental Hall effect measurements. The complex Fermi surface is built up by three major contributions. Two of them—in the vicinity of Γ and H points in reciprocal space (cf. Fig 4a)—are of n-type and one part shows hole character (near A point in Fig 4a). The calculation of the Hall coefficient $R_{H,calc}$ reveals that conductivity parallel to the basal plane of AlB_2 is governed by these hole type charge carriers. The corresponding value $R_{H,calc} = +8 \times 10^{-11}\,m^3/C$ confirms the sign and gives at least the same order of magnitude of the experimentally determined Hall coefficient. The numerical difference is caused by some simplifying assumptions used in our calculations like neglecting of defects in AlB_2 crystal structure as well as uniform relaxation time throughout the entire Fermi surface.

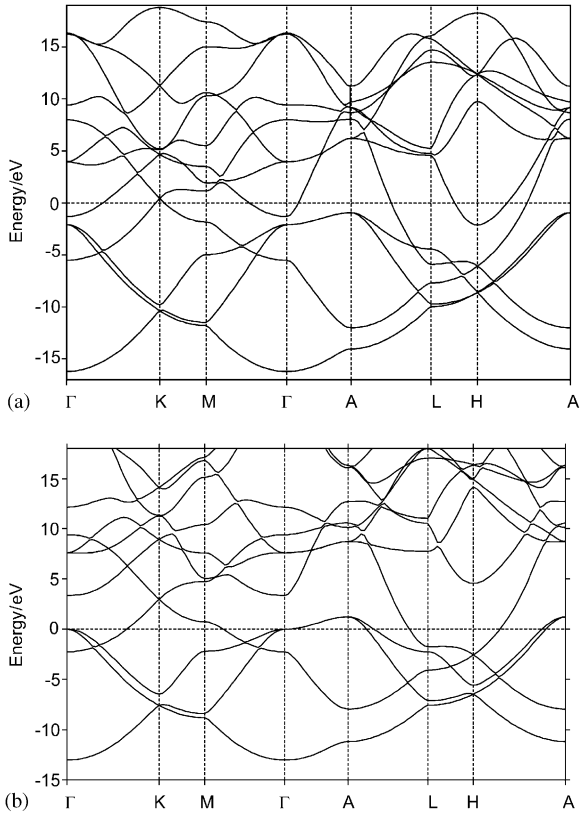

Fig. 4. (a) Band structure of stoichiometric aluminum diboride calculated by the LMTO method. (b) Band structure of hypothetical MgB_2 with the AlB_2 unit cell.

3.4. Chemical bonding

The electron localization function (ELF, η) was evaluated according to Refs. [20,21]. The isosurface for $\eta = 0.75$ (Fig. 5) reveals attractors on the B–B contacts in agreement with graphite-like net, but does not yield attractors above and below the boron atoms which would indicate π-interactions in a graphite-like model. The expected maxima seem to be split and displaced along Al–B contacts. This may indicate partially covalent character of the Al–B interaction. Applying the theory of gradient vector fields (procedure as proposed for the electron density [22]. The whole 3D field of ELF values can be divided into the basins of core attractors, bonding attractors and non-bonding attractors [23]. Integration of the electron density [24] within

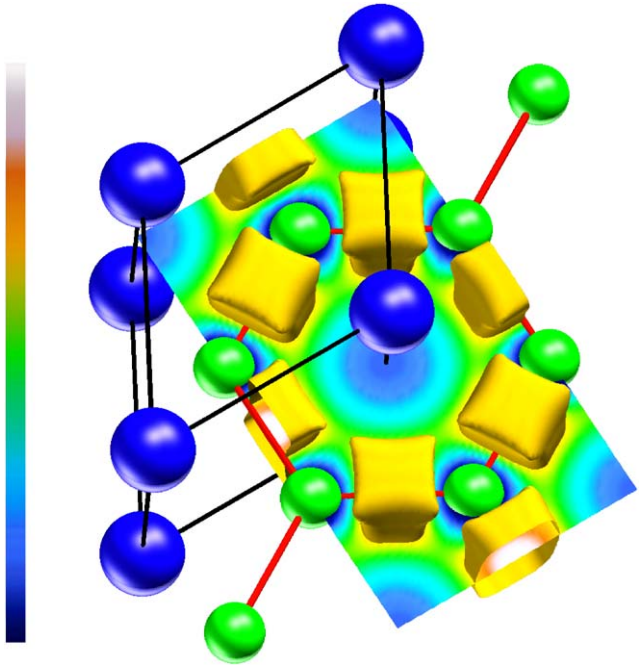

Fig. 5. Isosurface of the electron localization function ($\eta = 0.75$) of AlB_2 (blue, aluminum; green, boron; unit cell is given by black lines; view approximately along [001] direction).

these basins gives the number of electrons belonging to a respective attractor. Integration of the density of valence electrons in AlB_2 reveals 2.7 electrons per B–B attractor. This means that bonding is of the order 1.35. A similar calculation was performed for magnesium atoms at the aluminum site (for band structure see Fig. 4b). The electron density integration gives again 2.7 electrons per B–B bond. Thus, for the stabilization of the boron net only about four electrons per boron atom are necessary instead of 4.5 electrons available in stoichiometric AlB_2. Therefore, composition should be $(Al_{0.67})^{3+}(B_2)^{2-}$ according to the Zintl count. Apparently, additional electrons are responsible for metallic behavior of this material and for the (covalent) interaction between aluminum and boron atoms along [001] direction which means an excess of $(0.7e^-/f.u.)$ for the compound $(Al_{0.67+0.23})^{3+}(B_2)^{2-}$. Similar interaction between metal and boron was recently described for magnesium diboride [25, 26].

4. Conclusions

From X-ray single-crystal diffraction data, the crystals structure refinement of aluminum diboride (grown by the aluminum flux method) results defects on the aluminum position which corresponds to the composition $Al_{0.9}B_2$. This was confirmed by mass density and ^{11}B NMR measurements.

Electrical resistivity measured on a single crystal showed typical temperature dependence of a metal. Charge is carried dominantly by holes. p-type conductivity is confirmed by theoretical calculations.

Chemical bonding in aluminum diboride analyzed with the electron localization function indicates that the compound is not a Zintl phase but also may not achieve the ideal composition AlB_2.

References

[1] J. Nagamatsu, N. Nakagawa, T. Muranaka, Y. Zenitani, J. Akimitsu, Nature 410 (2001) 63–64.
[2] R. Cardoso Gil, W. Carrillo-Cabrera, M. Schultheiss, K. Peters, H.G. von Schnering, Yu. Grin, Z. Anorg. Allg. Chem. 625 (1999) 285–293;
H.G. von Schnering, U. Bolle, J. Curda, K. Peters, W. Carrillo-Cabrera, M. Somer, M. Schultheiss, U. Wedig, Angew. Chem. 108 (1996) 1062–1064;
H.G. von Schnering, U. Bolle, J. Curda, K. Peters, W. Carrillo-Cabrera, M. Somer, M. Schultheiss, U. Wedig, Angew. Chem. Int. Ed. 35 (1996) 984–986;
U. Bolle, W. Carrillo-Cabrera, K. Peters, H.G. von Schnering, Z. Kristallogr. NCS 213 (1998) 689.
[3] W. Hofmann, W. Jäniche, Naturwissenschaften 23 (1935) 851.
[4] V.I. Matkovich, J. Economy, R.F. Griese Jr., J. Am. Chem. Soc. 84 (1964) 2337–2340.
[5] W. Hofmann, W. Jäniche, Z. Physik. Chem. 31B (1936) 214–222.
[6] G.H. Funk, Z. Anorg. Allg. Chem. 142 (1925) 269–279.
[7] T.B. Massalski, H. Okamoto, P.R. Subramanian, L. Kacprzak, Binary Phase Diagrams, 2nd Edition, ASM International, 1990.
[8] V.N. Gurin, M.M. Korsukova, Prog. Crystal Growth Charact. 6 (1983) 59–101.
[9] S. Möhr, Hk. Müller-Buschbaum, Yu. Grin, H.G. von Schnering, Z. Anorg. Allg. Chem. 622 (1996) 1035–1037.
[10] J. Nakamura, M. Watanabe, T. Oguchi, S. Nasubida, E. Kabasawa, N. Yamada, K. Kuroki, H. Yamazaki, S. Shin, Y. Umeda, S. Minakawa, N. Kimura, H. Aoki, J. Phys. Soc. Japan 71 (2002) 408–410.
[11] I. Loa, K. Kunc, K. Syassen, P. Bouvier. Phys. Rev. B 66 (2002) 134101-1–134101-8.
[12] J.P. Kopp, R.G. Barnes, J. Chem. Phys. 54 (1971) 1840–1841.
[13] S.H. Baek, B.J. Suh, E. Pavarini, F. Borsa, R.G. Barnes, S.L. Bud'ko, P.C. Canfield, Phys. Rev. B 66 (2002) 104510-1–104510-7.
[14] E. Sirtl, L.M. Woerner, J. Crystal Growth 16 (1972) 215–218.
[15] O.K. Andersen, Phys. Rev. B 12 (1975) 3060–3083.
[16] O. Jepsen, A. Burkhardt, O.K. Andersen, The Program TB-LMTO-ASA, Version 4.7, Max-Planck-Institut für Festkörperforschung, Stuttgart, 1999.
[17] P.B. Allen, W.E. Pickett, H. Krakauer, Phys. Rev. B 37 (1988) 7482–7489.
[18] P.E. Blöchl, O. Jepsen, O.K. Andersen, Phys. Rev. B 49 (1994) 16223–16233.
[19] G. Lehmann, M. Taut, Phys. Stat. Sol. B 54 (1972) 469–477.
[20] A.D. Becke, K.E. Edgecombe, J. Chem. Phys. 92 (1990) 5397–5400;
A. Savin, A.D. Becke, J. Flad, R. Nesper, H. Preuss, H.G. von Schnering, Angew. Chem. 103 (1991) 421–424;
A. Savin, A.D. Becke, J. Flad, R. Nesper, H. Preuss, H.G. von Schnering, Angew. Chem. Int. Ed. 30 (1991) 409–412.
[21] A. Savin, O. Jepsen, J. Flad, O.K. Andersen, H. Preuss, H.G. von Schnering, Angew. Chem. 104 (1992) 186–188;
A. Savin, O. Jepsen, J. Flad, O.K. Andersen, H. Preuss, H.G. von Schnering, Angew. Chem. Int. Ed. 31 (1992) 187–188.
[22] R.F.W. Bader, Atoms in Molecules: A Quantum Theory, Oxford University Press, Oxford, 1990.
[23] B. Silvi, A. Savin, Nature 371 (1994) 683–686.
[24] M. Kohout, Program BASIN 2.2, User's Guide, M.Kohout@online.de, 2001.
[25] I.I. Mazin, O.K. Andersen, O. Jepsen, O.V. Kortus, A.A. Golubov, A.B. Kuzmenko, D. van der Marel, Phys. Rev. Lett. 89 (2002) 107002-1–107002-4.
[26] J. Schmidt, W. Schnelle, Yu. Grin, R. Kniep, Solid State Sci. 5 (2003) 535.
[27] L.G. Akselrud, P.Yu. Zavalii, Yu. Grin, V.K. Pecharsky, B. Baumgartner, E. Wölfel, Mater. Sci. Forum 133–136 (1993) 335–340.